



Science Arts & Métiers (SAM)

is an open access repository that collects the work of Arts et Métiers Institute of Technology researchers and makes it freely available over the web where possible.

This is an author-deposited version published in: <https://sam.ensam.eu>
Handle ID: <http://hdl.handle.net/10985/17032>

To cite this version :

Ilyes MNASSRI, Adil EL BAROUDI - Vibrational frequency analysis of finite elastic tube filled with compressible viscous fluid - Acta Mechanica Solida Sinica - Vol. 30, n°4, p.435-444 - 2017

Any correspondence concerning this service should be sent to the repository

Administrator : scienceouverte@ensam.eu



Vibrational frequency analysis of finite elastic tube filled with compressible viscous fluid

Ilyess Mnassri, Adil El Baroudi*

Arts et métiers ParisTech, Mechanics, 2 boulevard du Ronceray, BP 93525, France

ARTICLE INFO

Keywords:

Frequency analysis
Compressible Stokes flow
Coupled vibration
Elastodynamic

abstract

The vibrational frequency analysis of finite elastic tube filled with compressible viscous fluid has received plenty of attention in recent years. To apply frequency analysis to defect detection for example, it is necessary to investigate the vibrational behavior under appropriate boundary conditions. In this paper, we present a detailed theoretical study of the three-dimensional modal analysis of compressible fluid within an elastic cylinder. The dispersion equations of flexural, torsional and longitudinal modes are derived by elastodynamic theory and the unsteady Stokes equation. The symbolic software Mathematica is used in order to find the coupled vibration frequencies. The dispersion equation is deduced and analytically solved. The finite element results are compared with the present method for validation and an acceptable match between them are obtained.

1. Introduction

Wave propagation in liquid-filled elastic tubes since long has attracted the attention of engineers and scientists. One major application is blood flow through human arteries. Other studies involve applications in civil, oil and chemical industries, as well as biomedical and mechanical engineering.

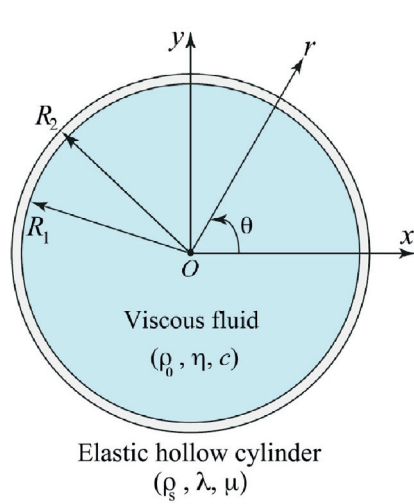
The firm basis of the theoretical models of wave propagation in fluid-filled elastic tubes is related to the work of Lamb and co-authors [1–3]. In addition, theoretical frequency analysis of viscous fluid motion has been developed by a large community of scientists. The fluid is commonly considered to be incompressible, which is valid for many cases of practical interest. It is therefore of fundamental interest to consider the case where the fluid compressibility is taken into account. This can be especially relevant to practical applications involving hydraulic fracturing. The understanding of wave propagation behavior in fluid-filled elastic tubes is of great inter-

est in engineering, geophysics and medicine [4–11]. Moreover, many studies have been conducted in the field of pipes conveying fluid, Zhou [12] studied the motion of ring-stiffened thin-walled cylindrical shells conveying fluid, and showed that the natural frequencies and the corresponding critical fluid velocity increase in pair with Young modulus, size, or number of the stiffeners. Zhang et al. [13] used vibration analysis to investigate the fluid transmission through carbon nanotube using the nonlocal elastic theory, and calculated the first five orders of natural frequency of the carbon nanotube. Zhang et al. [14] showed that fluid-conveying carbon nanotube forest with crossed distributions is very efficient in acoustic wave absorption. Hosseini and Bahaadini [15] evinced that the modified strain gradient theory predicts more natural frequencies and more flutter critical speeds than the modified couple stress theory for cantilever micro-pipes conveying fluid.

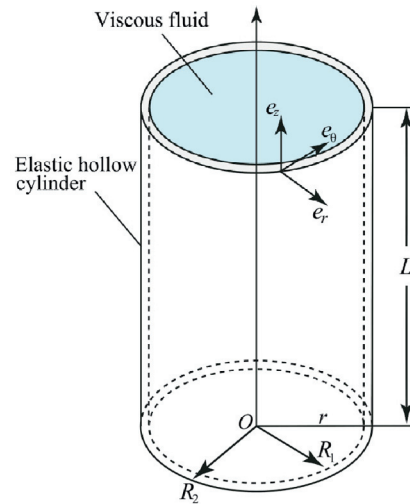
The motivation of this work is to provide a theoretical three-dimensional study that can be regarded as a benchmark model. Predicting and understanding frequency analysis in fluid-filled elastic tubes are of significant importance because they are often used in the detection of fracture characteristics [4–6,16].

* Corresponding author.

E-mail address: adil.elbaroudi@ensam.eu (A.E. Baroudi).



(a) Cross section of the system.



(b) Three-dimensional geometry.

Fig. 1 – The geometry of fluid-filled elastic tube.

The frequency analysis of a viscous fluid can be dramatically affected by the properties of the solid in which it is confined. Although calculation of the natural frequencies in rigid solid can be performed routinely, analysis of the effects of elastic solid poses a formidable challenge. Importantly, a theoretical model for the frequency analysis of fluid-filled elastic tubes, which exhibits these modes of deformation, knowledge and understanding of the involved physical processes, is lacking at present.

In this contribution, we investigate the vibrational behavior of a compressible fluid within an elastic cylinder, which describes the interrelation between the fluid's density and viscosity. For a compressible viscous fluid problem, the exact formulation is based upon a convenient decomposition of the velocity field into three contributions, with one related to the scalar potential, and the other two being vector potentials. The solutions of the differential equations of motion turn out to be complex, and can be conveniently treated with the aid of the symbolic software Mathematica. Furthermore, this work investigates the influence of length-radius aspect ratio on the vibrational behavior. The finite element results are compared with the present method for validation. One of our aims behind this study is the attention to use the numerical formulation in the future for more general geometries.

2. Governing equations

2.1. Fluid formulation

To get a general mathematical formulation of wave propagation in viscous medium, the dynamics for compressible fluid is considered. Fig. 1 shows the coordinate configuration of wave propagation in viscous compressible homogeneous fluid confined by an elastic solid. The amplitude of oscillation is considered to be sufficiently small so that convective inertial

forces in the fluid can be neglected. This implies that the fluid dynamics can be modeled as an unsteady linear Stokes flow. Assuming that the fluid is Newtonian, its constitutive equation is given by

$$\mathbf{T} = \left(-p - \frac{2\eta}{3} \nabla \cdot \mathbf{v} \right) \mathbf{I} + \eta \left[\nabla \mathbf{v} + (\nabla \mathbf{v})^T \right] \quad (1)$$

where \mathbf{I} is a unit tensor, η is the dynamic viscosity, p is the fluid pressure, $\mathbf{v} = \{v_r, v_\theta, v_z\}^T$ is the fluid velocity vector, ρ is the density of fluid and \mathbf{T} the total fluid stress tensor (pressure and viscous forces). From conservations of mass and momentum, the linearized Navier–Stokes equations of motion of viscous compressible fluid specialized for small amplitudes of velocities in the absence of body force is governed by (see [17])

$$\frac{\partial \rho}{\partial t} + \nabla \cdot (\rho \mathbf{v}) = 0 \quad (2)$$

$$\rho \frac{\partial \mathbf{v}}{\partial t} = -\nabla p + \eta \nabla^2 \mathbf{v} + \frac{\eta}{3} \nabla \nabla \cdot \mathbf{v} \quad (3)$$

When fluid experiences a disturbance with small amplitude, its ambient physical variables are modified as $\mathbf{v} = \mathbf{v}'$, $p = p'$, $\rho = \rho_0 + \rho'$, where ρ_0 is constant. The primed quantities \mathbf{v}' , p' and ρ' represent small changes in flow velocity, pressure and density, respectively. To first order the small quantities above, substituting the modified variables into Eqs. (2) and (3), and dropping all primes for convenience, we have

$$\frac{\partial \rho}{\partial t} + \rho_0 \nabla \cdot \mathbf{v} = 0 \quad (4)$$

$$\rho_0 \frac{\partial \mathbf{v}}{\partial t} = -\nabla p + \eta \nabla^2 \mathbf{v} + \frac{\eta}{3} \nabla \nabla \cdot \mathbf{v} \quad (5)$$

For acoustic problems, we assume that a small change in ρ induces small changes in p by fast adiabatic processes. Under the assumption of the constant entropy s of fluid in wave propagation, the isentropic equation of state can be expressed

by $p = \rho(\partial p / \partial \rho)_s = \rho c^2$, where the adiabatic sound velocity $c = c(p, \rho)$ is a function of pressure and density. Substituting this into Eq. (4) gives

$$\frac{\partial p}{\partial t} + c^2 \rho_0 \nabla \cdot \mathbf{v} = 0 \quad (6)$$

Multiplying the $\partial/\partial t$ to both sides of Eq. (6) and then inserting in Eq. (5), we get

$$\rho_0 \frac{\partial^2 \mathbf{v}}{\partial t^2} = \left(c^2 \rho_0 + \frac{\eta}{3} \frac{\partial}{\partial t} \right) \nabla \nabla \cdot \mathbf{v} + \eta \frac{\partial}{\partial t} (\nabla^2 \mathbf{v}) \quad (7)$$

A solution to Eqs. (4) and (5) can be obtained by decomposing the velocity field into its curl-free and divergence-free components, namely [18]

$$\mathbf{v} = \nabla \phi + \nabla \times (\psi \mathbf{e}_z) + \nabla \times \nabla \times (\chi \mathbf{e}_z) \quad (8)$$

where ϕ, ψ and χ are scalar potentials, and \mathbf{e}_z is the unit vector along the axial coordinate. Insertion of this into Eq. (5) yields

$$\nabla^2 \psi - \frac{1}{\nu} \frac{\partial \psi}{\partial t} = 0, \quad \nabla^2 \chi - \frac{1}{\nu} \frac{\partial \chi}{\partial t} = 0 \quad (9)$$

and

$$p = \eta \left(\frac{4}{3} \nabla^2 \phi - \frac{1}{\nu} \frac{\partial \phi}{\partial t} \right) \quad (10)$$

To obtain the wave equation for scalar potential ϕ , we insert Eq. (8) into (7), so that

$$\left(c^2 + \frac{4\eta}{3\rho_0} \frac{\partial}{\partial t} \right) \nabla^2 \phi - \frac{\partial^2 \phi}{\partial t^2} = 0 \quad (11)$$

Introducing a new auxiliary variable $\alpha = j\sqrt{j\omega/\nu}$ (is the complex wavenumber) and using previously developed techniques [19,20], the solution describing the scalar potential ϕ of the damped wave equation, i.e. Eq. (11), can be expressed as

$$\phi(r, \theta, z, t) = A I_n(k_\phi r) \sin(n\theta) \cos(k_z z) e^{j\omega t} \quad (12)$$

where ω is the angular frequency. A similar solution of the two remaining subequations of Eq. (9) can be obtained as

$$\begin{aligned} \psi(r, \theta, z, t) &= B J_n(k_\psi r) \cos(n\theta) \cos(k_z z) e^{j\omega t} \\ \chi(r, \theta, z, t) &= C J_n(k_\psi r) \sin(n\theta) \sin(k_z z) e^{j\omega t} \end{aligned} \quad (13)$$

The fluid nodes at the two ends are constrained in the global z-displacement with $v_z = 0$, and the tube is simply supported at the two ends with $u_z = 0$. For this two conditions, it can be easily shown that the axial wave number k_z is a function of axial mode m and tube length L as $k_z = m\pi/L$ (k_z is found by satisfying $v_z = 0$ and $u_z = 0$ at $z = 0$ and $z = L$). In the above equations, ν is the kinematic viscosity of fluid, n is the circumferential order of the respective guided mode, k_ϕ is the modified wavenumber associated with the dilatational wave in fluid, k_ψ is the modified wavenumber associated with the shear wave in fluid, I_n is an n th order modified Bessel function of the first kind, J_n is an n th order Bessel function of the first kind, and A, B and C are unknown wave propagation coefficients whose solutions are to be determined from boundary

conditions. The modified dilatational and shear wavenumbers are calculated using

$$k_\phi^2 = \frac{\alpha^2}{\left(\frac{c}{\nu\alpha}\right)^2 - \frac{4}{3}} + k_z^2, \quad k_\psi^2 = \alpha^2 - k_z^2$$

Note that when the radial wavenumber k_ψ is taken equal to zero, the parameter $\text{Im}(\nu k_z^2)$ is a resonance frequency parameter. The frequencies are the cut-off frequencies and can be plotted as functions of ν , for different values of the longitudinal wavenumber m . For the remainder of this article, the exponential term with respect to time is suppressed in all of the equations. Thus, the acoustic pressure can be obtained by insertion of Eq. (13) into Eq. (11)

$$p(r, \theta, z) = \frac{4\eta}{3} \left(k_\phi^2 - k_z^2 + \frac{3\alpha^2}{4} \right) A I_n(k_\phi r) \sin(n\theta) \cos(k_z z) \quad (14)$$

Hence, the velocity field can be determined from Eqs. (8), (12) and (13) in the form

$$\begin{Bmatrix} v_r \\ v_\theta \\ v_z \end{Bmatrix} (r, \theta, z) = \begin{Bmatrix} v_r(r) \sin(n\theta) \cos(k_z z) \\ v_\theta(r) \cos(n\theta) \cos(k_z z) \\ v_z(r) \sin(n\theta) \sin(k_z z) \end{Bmatrix} \quad (15)$$

where the radial dependence is defined as

$$\begin{aligned} v_r(r) &= \phi'(r) - \frac{n}{r} \psi(r) + k_z \chi'(r) \\ v_\theta(r) &= \frac{n}{r} \phi(r) - \psi'(r) + \frac{nk_z}{r} \chi(r) \\ v_z(r) &= -k_z \phi(r) + k_\psi^2 \chi(r) \end{aligned}$$

and the prime signifies the differentiation with respect to the argument r . Note that the velocity field \mathbf{v} has components that are symmetric or antisymmetric in θ and z . Following standard practice, the solutions with symmetric (antisymmetric) axial velocities are called the antisymmetric (symmetric) axial modes, respectively, with k_z^a and k_z^s denoting the corresponding eigenvalues. Thus, we have $k_z^a = (m-1)\pi/L$ and $k_z^s = m\pi/L$. However, the azimuthal modes corresponding to $\cos(n\theta)$ and $\sin(n\theta)$ are exactly the same due to periodicity in the azimuthal direction, i.e. there is no distinction in the values of n between the two families. Consequently, direct substitution of the expansions of Eqs. (14) and (15) into the stress-velocity relations of Eq. (1) with some manipulations leads to

$$\begin{Bmatrix} T_{rr} \\ T_{r\theta} \\ T_{rz} \end{Bmatrix} (r, \theta, z) = \begin{Bmatrix} T_{rr}(r) \sin(n\theta) \cos(k_z z) \\ T_{r\theta}(r) \cos(n\theta) \cos(k_z z) \\ T_{rz}(r) \sin(n\theta) \sin(k_z z) \end{Bmatrix} \quad (16)$$

where the radial dependence is defined as

$$\begin{aligned} T_{rr}(r) &= 2\eta \left\{ \phi''(r) - \left(k_\phi^2 - k_z^2 + \frac{\alpha^2}{2} \right) \phi(r) - \frac{n}{r^2} [r\psi'(r) - \psi(r)] + k_z \chi''(r) \right\} \\ T_{r\theta}(r) &= \eta \left\{ \frac{2n}{r^2} [r\phi'(r) - \phi(r)] - 2\psi''(r) - k_\psi^2 \psi(r) + \frac{2nk_z}{r^2} [r\chi'(r) - \chi(r)] \right\} \\ T_{rz}(r) &= \eta \left\{ -2k_z \phi'(r) + \frac{nk_z}{r} \psi(r) + (k_\psi^2 - k_z^2) \chi'(r) \right\} \end{aligned}$$

2.2. Circular elastic cylinder

The simply-supported cylinder under consideration is assumed to be made of linearly elastic homogeneous and isotropic material. In order to derive the PDE for structural mechanics, we decompose the displacement field u as the sum of the gradient of a scalar potential and the curl of a vector potential. In the absence of body forces, the equation describing the motion is governed by [18]

$$\nabla^2 \Phi - \frac{\nu^2 \alpha^4}{c_l^2} \Phi = 0, \quad \nabla^2 \Psi - \frac{\nu^2 \alpha^4}{c_t^2} \Psi = 0, \quad \nabla^2 \Theta - \frac{\nu^2 \alpha^4}{c_t^2} \Theta = 0 \quad (17)$$

where $c_l = \sqrt{(\lambda + 2\mu)/\rho_s}$ and $c_t = \sqrt{\mu/\rho_s}$ are the compression and shear wave velocities in the elastic cylinder, respectively. (λ, μ) are Lamé constants, ρ_s is the density, and (Φ, Ψ, Θ) are scalar potential functions. Using previously developed techniques [19,20], the solution of three wave equations, i.e. Eq. (17), can be obtained as follows

$$\begin{Bmatrix} \Phi \\ \Psi \\ \Theta \end{Bmatrix}_{r,\theta,z} = \begin{Bmatrix} \Phi(r) \\ \Psi(r) \\ \Theta(r) \end{Bmatrix}_{\theta,z} = \begin{Bmatrix} [A_1 I_n(k_\Phi r) + A_2 K_n(k_\Phi r)] \sin(n\theta) \cos(k_z z) \\ [B_1 I_n(k_\Psi r) + B_2 K_n(k_\Psi r)] \cos(n\theta) \cos(k_z z) \\ [C_1 I_n(k_\Psi r) + C_2 K_n(k_\Psi r)] \sin(n\theta) \sin(k_z z) \end{Bmatrix} \quad (18)$$

where K_n is an n th order standard modified Bessel function of the second kind, and the unknown coefficients $A_1, A_2, B_1, B_2, C_1, C_2$ are to be determined from boundary conditions. The modified dilatational and shear wave numbers in the elastic cylinder are calculated using $k_\Phi^2 = \frac{\nu^2 \alpha^4}{c_l^2} + k_z^2$ and $k_\Psi^2 = \frac{\nu^2 \alpha^4}{c_t^2} + k_z^2$. Furthermore, the displacement components of the elastic cylinder can be written as

$$\begin{Bmatrix} u_r \\ u_\theta \\ u_z \end{Bmatrix} = \begin{Bmatrix} u_r(r) \\ u_\theta(r) \\ u_z(r) \end{Bmatrix}_{\theta,z} = \begin{Bmatrix} [\Phi'(r) - \frac{n}{r} \Psi(r) + k_z \Theta'(r)] \sin(n\theta) \cos(k_z z) \\ [\frac{n}{r} \Phi(r) - \Psi'(r) + \frac{nk_z}{r} \Theta(r)] \cos(n\theta) \cos(k_z z) \\ [-k_z \Phi(r) - k_\Psi^2 \Theta(r)] \sin(n\theta) \sin(k_z z) \end{Bmatrix} \quad (19)$$

Then, the pertinent stress components can be obtained as follows

$$\begin{Bmatrix} \sigma_{rr} \\ \sigma_{r\theta} \\ \sigma_{rz} \end{Bmatrix} = \begin{Bmatrix} \sigma_{rr}(r) \sin(n\theta) \cos(k_z z) \\ \sigma_{r\theta}(r) \cos(n\theta) \cos(k_z z) \\ \sigma_{rz}(r) \sin(n\theta) \sin(k_z z) \end{Bmatrix} \quad (20)$$

where the radial dependence is defined as

$$\begin{aligned} \sigma_{rr}(r) &= \mu \left\{ 2\Phi''(r) + \frac{\lambda \nu^2 \alpha^4}{\mu c_l^2} \Phi(r) - \frac{2n}{r^2} [r\Psi'(r) - \Psi(r)] + k_z \Theta''(r) \right\} \\ \sigma_{r\theta}(r) &= \mu \left\{ \frac{2n}{r^2} [r\Phi'(r) - \Phi(r)] - 2\Psi''(r) + k_\Psi^2 \Psi(r) + \frac{2nk_z}{r^2} [r\Theta'(r) - \Theta(r)] \right\} \\ \sigma_{rz}(r) &= \mu \left\{ -2k_z \Phi'(r) + \frac{nk_z}{r} \Psi(r) - (k_\Psi^2 + k_z^2) \Theta'(r) \right\} \end{aligned}$$

3. Boundary conditions

In the solid-fluid interface problems, the normal stress of the elastic cylinder is equal to the normal stress of the fluid, and the displacement (velocity) of the elastic cylinder is equal to the displacement (velocity) of the fluid. These conditions are due to the continuity of the stresses and displacement of the solid and fluid on the curved boundaries. Thus the relevant boundary conditions which must be imposed at the inner and outer surfaces of the hollow cylinder in contact with the viscous compressible fluid medium are as follows:

■ continuity of the velocity (displacement) of the solid and fluid at $r = R_1$

$$v_r(r) + \nu \alpha^2 u_r(r) = 0, \quad v_\theta(r) + \nu \alpha^2 u_\theta(r) = 0, \quad v_z(r) + \nu \alpha^2 u_z(r) = 0 \quad (21)$$

■ continuity of the normal stresses of the solid and fluid at $r = R_1$

$$T_{rr}(r) - \sigma_{rr}(r) = 0, \quad T_{r\theta}(r) - \sigma_{r\theta}(r) = 0, \quad T_{rz}(r) - \sigma_{rz}(r) = 0 \quad (22)$$

■ stress-free surface at $r = R_2$

$$\sigma_{rr}(r) = 0, \quad \sigma_{r\theta}(r) = 0, \quad \sigma_{rz}(r) = 0 \quad (23)$$

Finally, making use of the expansions in Eqs. (15), (16), (19) and (20) in the above boundary conditions, we obtain a linear system of equations in terms of the unknown coefficients $A, B, C, A_1, A_2, B_1, B_2, C_1$ and C_2 of the general form

$$[\mathbf{M}] \{A \ B \ C \ A_1 \ A_2 \ B_1 \ B_2 \ C_1 \ C_2\}^T = \{0 \ 0 \ 0 \ 0 \ 0 \ 0 \ 0 \ 0\}^T \quad (24)$$

where $[\mathbf{M}]$ is a 9×9 matrix and is given in the Appendix. For the non-trivial solution, the determinant of this set of equations must be zero.

3.1. Torsional and longitudinal modes

Eq. (24) can be solved for the eigenvalues k_z at a fixed circumferential order $n=0, 1, \dots$ and selected angular frequency ω . The solutions for $n=0$ correspond to the longitudinal modes $L(0, m)$, together with the torsional modes $T(0, m)$. The solutions for $n=1$ correspond to the flexural modes $F(1, m)$, and the lobar modes correspond to $n > 1$.

3.1.1. Torsional modes $T(0, m)$

The torsional modes correspond to a circumferential order $n=0$, for which the displacements u_r and u_z (velocities v_r and v_z) are both zero and only the circumferential displacement $u_\theta \neq 0$ (velocity $v_\theta \neq 0$) is independent of the circumferential coordinate θ . In this case the boundary conditions for Eqs. (21)–(23) become

$$v_\theta(R_1) + \nu \alpha^2 u_\theta(R_1) = 0, \quad T_{r\theta}(R_1) - \sigma_{r\theta}(R_1) = 0, \quad \sigma_{r\theta}(R_2) = 0$$

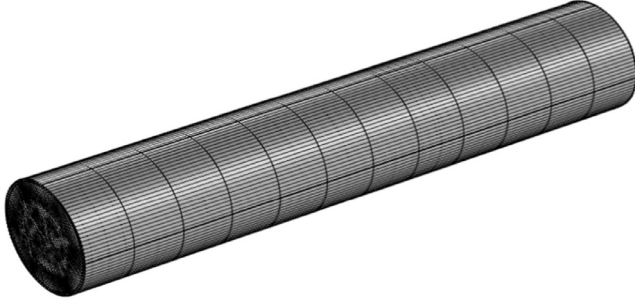


Fig. 2 – FE model of finite elastic tube filled with viscous fluid.

Then, Eq. (24) becomes

$$[\mathbf{M}_t] \{B \ B_1 \ B_2\}^T = \{0 \ 0 \ 0\}^T \quad (25)$$

Solving $\det[\mathbf{M}_t] = 0$ gives the torsional modes.

3.1.2. Longitudinal modes $L(0, \mathbf{m})$

The longitudinal modes correspond to a circumferential order $n = 0$ with the absence of torsional displacement $u_\theta = 0$ (velocity $v_\theta = 0$). In this case the boundary conditions for Eqs. (21)–(23) become

$$T_{rr}(R_1) - \sigma_{rr}(R_1) = 0, \quad T_{rz}(R_1) - \sigma_{rz}(R_1) = 0$$

$$v_r(R_1) + \nu \alpha^2 u_r(R_1) = 0, \quad v_z(R_1) + \nu \alpha^2 u_z(R_1) = 0$$

$$\sigma_{rr}(R_2) = 0, \quad \sigma_{rz}(R_2) = 0$$

Then, Eq. (24) becomes

$$[\mathbf{M}_l] \{A \ C \ A_1 \ A_2 \ C_1 \ C_2\}^T = \{0 \ 0 \ 0 \ 0 \ 0 \ 0\}^T \quad (26)$$

Solving $\det[\mathbf{M}_l] = 0$ gives the longitudinal modes.

3.2. Finite element modeling

In this section, the commercially available FEA package COMSOL Multiphysics is used to develop the finite element model of vibrational frequency analysis of finite elastic tube filled with compressible viscous fluid (Fig. 2). This modeling procedure requires two modules: one for simulating the elastic tube and the other for viscous fluid. Each module provides a wide range of equations, which is needed in specifying sub-domains and boundaries. The theories and equations behind this model are based on the governing equations in Section 2. The tube is considered to be a three dimensional solid, stress-strain problem. The elastic tube and fluid are simulated using the Lagrange-Quadratic element and Lagrange-P2P1 element, respectively. The tube and fluid elements at the interface share the same node and have extremely fine meshing to capture the details during coupled vibrations. The applied boundary conditions are as follows. The tube is simply-supported at two ends ($u_z = 0$). The fluid nodes at the two ends are constrained in the global z-displacement ($v_z = 0$).

The complete coupled system is simulated and presented in this section. Two modules (Fluid Flow and Structural Mechanics) are used in this simulation. An elastic cylinder is used to envelope the fluid domain. On the outer cylindrical perimeter of the solid domain, free constraint condition is used. The coupling of elastic tube vibration with viscous fluid inside the tube is performed using both the Fluid Flow and Structural Mechanics modules. For this purpose, some variables are set to make the connection between these two modules. At fluid-structure interface kinematic and dynamic continuity has to be ensured. The complete coupled problem has to fulfill the condition that the location of the fluid-structure interface coincides for both fields. Thus, the fluid-structure interaction boundary condition concerning the fluid is of an inhomogeneous Dirichlet type (kinematic condition) representing mass conservation across the interface, and the fluid-structure boundary condition for the solid is given by an inhomogeneous Neumann condition (dynamic condition) describing the equivalence of fluid stresses and solid stresses in the normal direction. For modeling of the coupled system, the eigenfrequency solver and analysis are selected to solve the model and give the first eight eigenvalues. According to this solver, time for solving the model is 6.829 min and the number of degrees of freedom is 361,392.

4. Results' validation and discussion

We consider the circular elastic cylinder filled with a compressible viscous fluid, as shown in Fig. 1, and assume that the radius of the internal circle of the inner cylinder is $a = R_1$ and the radius of the external circle is R_2 . The resulting frequency equations of the lobar, flexural, longitudinal and torsional modes given in Eq. (24) are transcendental in nature with respect to the frequency ω . To obtain the roots of the frequency equation, the Mathematica software is used. In this study we use an elastic cylinder with Young's modulus $E = 10 \times 10^9$ Pa, Poisson's ratio $\nu_s = 0.3$, and density $\rho_s = 2750$ kg/m³. The fluid used in the cylinder has a density of 1000 kg/m³ and a dynamic viscosity of 0.001 Pa s. With the derived eigenfrequency equations, natural frequencies ω are calculated using the software Mathematica. The natural frequencies are computed directly from the determinant of Eq. (24). To validate the analytical results, the natural frequencies and mode shapes are also

Table 1 – The first eight coupled eigenvalues ω .

$L/a = 4$			$L/a = 8$			$L/a = 12$		
(n, m)	Exact	FEM	(n, m)	Exact	FEM	(n, m)	Exact	FEM
(1,2)	14.07	14.07	(1,3)	14.00	14.00	(1,5)	13.98	13.98
(1,1)	14.22	14.22	(1,4)	14.07	14.07	(1,4)	14.05	14.05
(0,1)	15.29	15.29	(1,2)	14.22	14.22	(1,6)	14.07	14.07
(1,3)	15.50	15.50	(1,1)	14.53	14.53	(1,3)	14.22	14.22
(0,2)	17.15	17.15	(1,5)	14.56	14.56	(1,7)	14.34	14.34
(1,4)	18.71	18.71	(0,1)	14.83	14.83	(1,2)	14.44	14.44
(0,3)	20.23	20.23	(0,2)	15.29	15.29	(1,1)	14.61	14.61
(1,5)	23.54	23.54	(1,6)	15.50	15.50	(0,1)	14.75	14.75

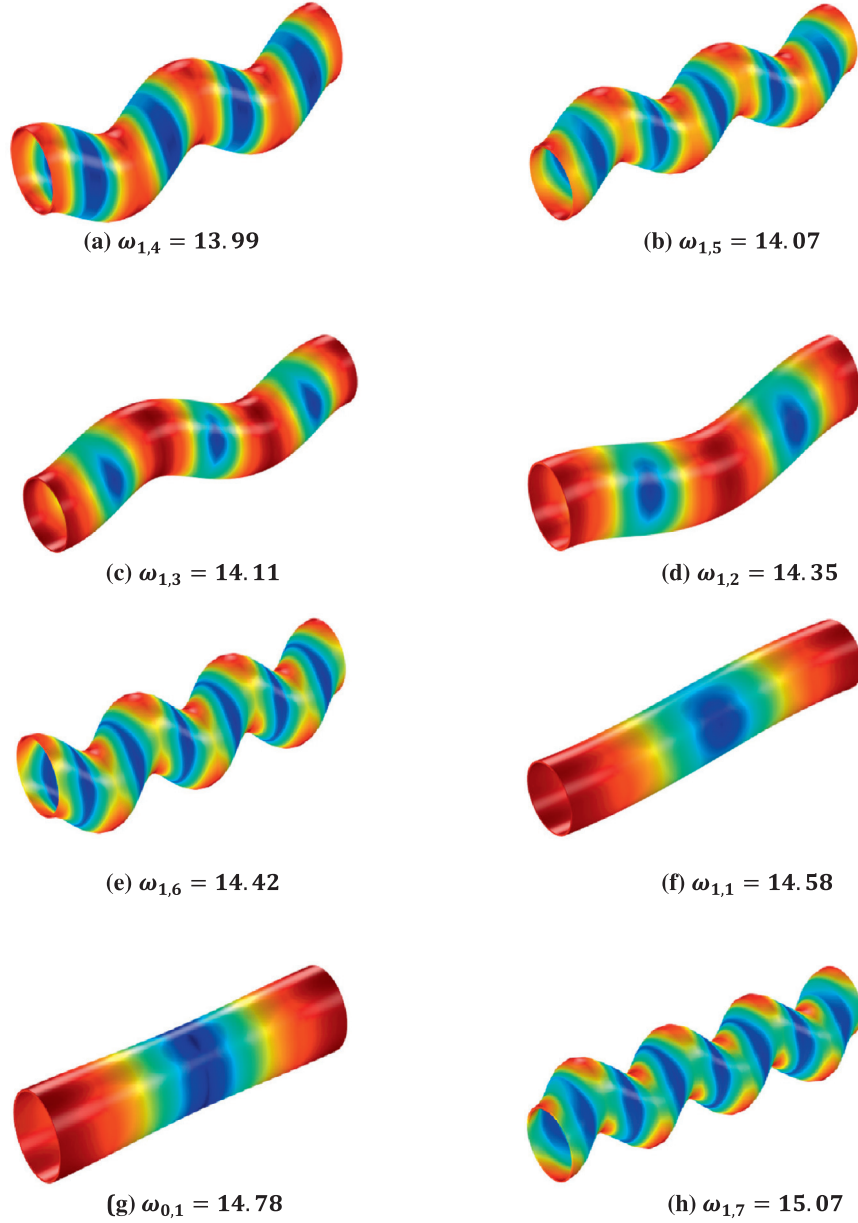


Fig. 3 – First eight angular frequencies $\omega_{n,m}$ and associated mode shapes ($L/a = 10$). (0,1) corresponds to torsional modes and (1, m) corresponds to flexural modes.

computed using Comsol Multiphysics FEM Simulation Software [21]. A very good agreement is observed between the results of the present method and those of the FEM.

To study the dependence of ω on the geometric ratio of the cylinder, we plot the normalized frequency, $\omega a^2/\nu$, against L/a in Figs. 6–8 for L/a ranging from 2 to 16. In these figures, we set $a = 1$ mm with a varying value of L . The dispersion curves for the vibration modes $F(1, m)$, $T(0, m)$ and $L(0, m)$ are given in Figs. 6–8, respectively. Only the first four longitudinal modes (i.e., $m = 1, 2, 3, 4$) are shown. Note that there is more than one root for the natural angular frequency for a fixed set of n and m because of the nonlinearity of ω involved in the frequency equation.

For the natural frequencies of compressible viscous fluid within an elastic cylinder, the following concluding remarks can be drawn:

- The frequencies given in Table 1 are restricted to circular cylinders with $L/a = 4, 8, 12$. To study the dependence of frequencies on the geometric ratio of the cylinder, we plot the normalized frequency, $\omega a^2/\nu$, against L/a in Figs. 6–8. The dependence of frequencies $\omega a^2/\nu$ upon the ratio L/a is clearly illustrated. This behavior is also found for $m \geq 5$. Fig. 7 also shows that all the torsional modes are dispersive except for the mode $T(0, 0)$. The mode $T(0, 0)$ corresponds to an in-plane vibration.

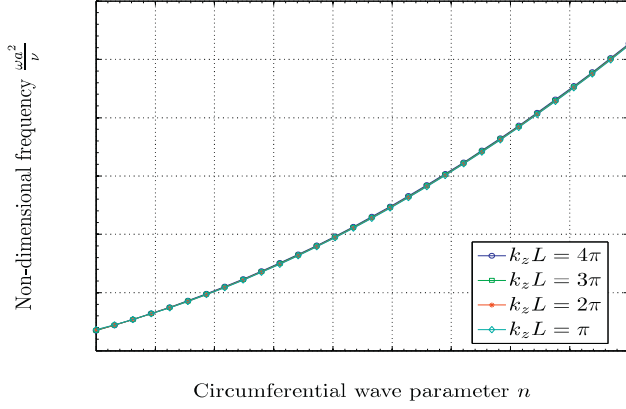


Fig. 4 – Dispersion curves with $\omega a^2/\nu$ against n for $m = 1, 2, 3, 4$.

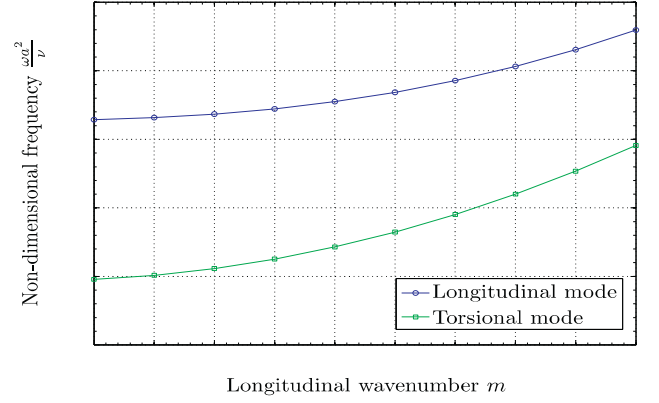


Fig. 5 – Dispersion curves with $\omega a^2/\nu$ against m for longitudinal and torsional modes.

- Fig. 3 illustrates the first eight mode shapes. The mode shape can be regarded as the mode (n, m) , where n is the modal number in the circumferential direction and m is the modal number in the axial direction. The modal shapes in Fig. 3 are not in order with the parameters n and m ; for example, the frequency of mode $(1, 3)$ is lower than that of mode $(1, 1)$. This feature of thin cylinder vibration is different from that of beam vibration, in which the order increases with the modal parameter. Therefore, one should be careful to find the right mode for shell vibration.
- In Fig. 4, we begin by examining how the non-dimensional frequencies for the given L/a ratio vary with the axial mode m and the circumferential mode n . The non-dimensional frequencies increase as the circumferential mode n increases. Fig. 4 shows an interesting results established by the fact that the four $k_z L$ frequency curves are superposed, which means that the non-dimensional frequencies are only determined by n and are regardless of the axial mode m . For a given n the frequency increases as m increases. Therefore, the fundamental frequency is not always with the $m=1$ curve. In the following we study the frequency curves of $m=1, 2, 3, 4$ with changes of the other cylinder parameters.
- Fig. 5 shows how the non-dimensional frequencies for longitudinal and torsional modes vary with the axial mode. The non-dimensional frequencies increase as the axial mode m increases. The difference between longitudinal and torsional modes reduces as the axial mode m increases.
- It is easy to observe from Fig. 6 that the frequency dispersion curves do not intersect each other when L/a is smaller than 4. It is noted that the frequency spectrum for the lobar modes ($n \geq 2$) has a behavior similar to the flexural modes $F(1, m)$.
- The cut-off frequencies are given in Fig. 9. These are the frequencies below which some types of wave cannot travel, and they correspond to the wave speeds which approach infinity as the wavenumber approaches zero. This figure shows how these frequencies vary with the L/a ratio. The frequencies decrease significantly with the increase of L/a ratio. By comparing Figs. 6–8 with Fig. 9, we know that the

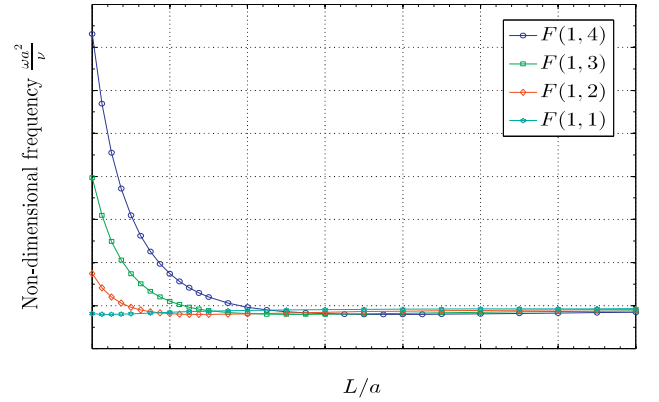


Fig. 6 – Dispersion curves with $\omega a^2/\nu$ against L/a for flexural modes.

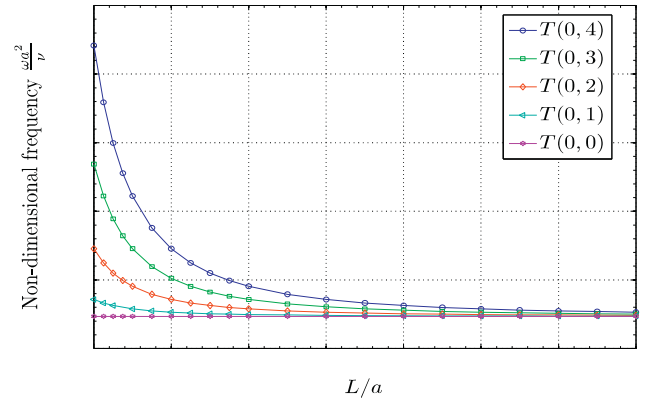


Fig. 7 – Dispersion curves with $\omega a^2/\nu$ against L/a for torsional modes.

cut-off frequency is different from that of the corresponding mode.

- Finally, one investigates how the fluid's compressibility affects the natural frequencies. Fig. 10 shows the coupled natural frequencies, varying with the circumferential wavenumber n for flexural ($n=1$) and lobar ($n \geq 2$) modes.

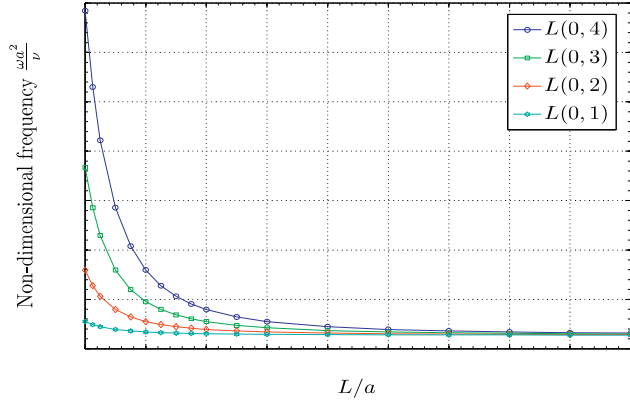


Fig. 8 – Dispersion curves with $\omega a^2/\nu$ against L/a for longitudinal modes.

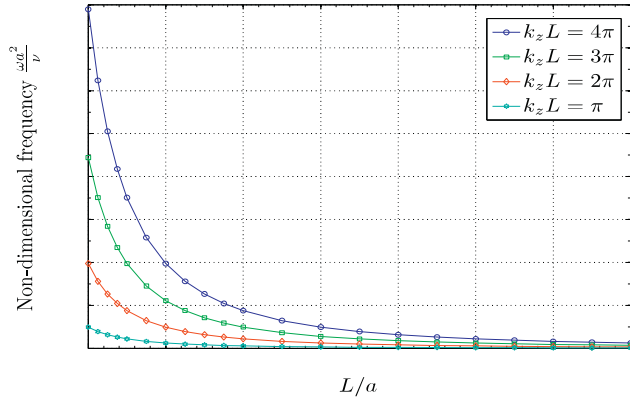


Fig. 9 – The cut-off frequency dispersion curves with $\omega a^2/\nu$ against L/a .

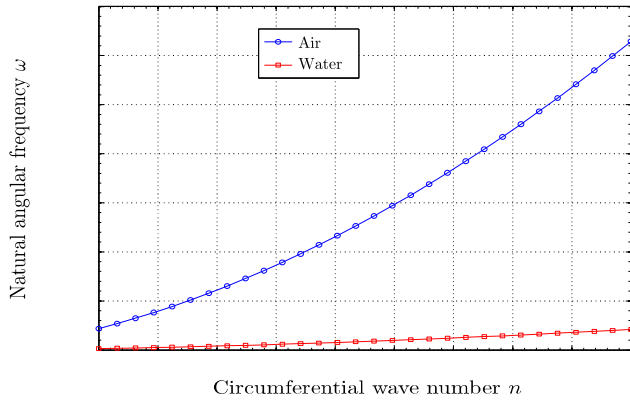


Fig. 10 – The frequency dispersion curves with ω against n for $k_z L = \pi$.

As expected, it is clearly stated that when n increases, the difference between air and water frequencies increases. This behavior is also found for other modes (i.e., longitudinal and torsional ones (see Figs. 11 and 12). Fluid's compressibility may be neglected in the case of water. However, compressibility cannot be neglected in the case of air.

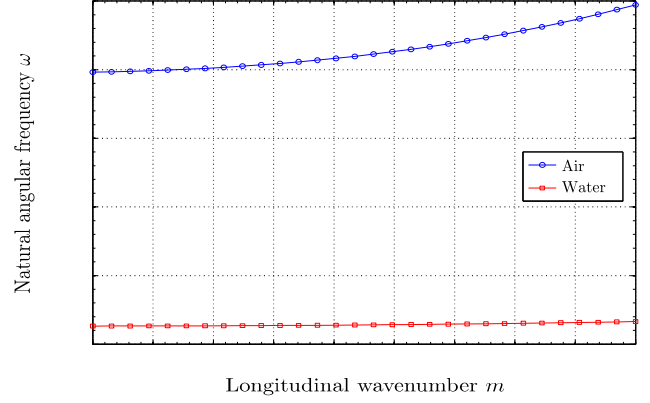


Fig. 11 – The longitudinal frequency dispersion curves with ω against m .

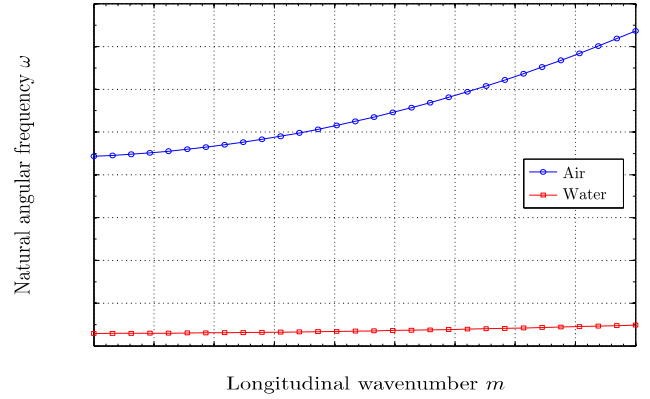


Fig. 12 – The torsional frequency dispersion curves with ω against m .

5. Conclusion

An exact approach based on the linear three-dimensional elasticity theory is used to determine the dispersion curves of compressible viscous fluid within an elastic tube. The governing equations are solved to obtain the exact frequency equation, which are presented for coupled problem. The results obtained in this paper can serve as a benchmark solution and as a reference to assess the accuracy of approximate methods. High accuracy has been observed in the analysis. For demonstration, the natural frequencies of length-radius vs. frequency parameters for various mode categories are given. Three analytical formulations are presented for the lobar ($n \geq 2$, m), flexural $F(1, m)$, longitudinal $L(0, m)$ and torsional $T(0, m)$ modes. These modes are involved separately in most practical applications and users can implement only the required equations. The validity of the present solution is confirmed numerically. Additionally, the study of thermal coupling effect should be explored in future work.

Appendix

The below formulas may expediently be utilized to obtain the elements of the matrix given in Eq. (24):

$$\{\mathbf{X}\}_{\text{fluid}} = [\mathbf{N}]_{\text{fluid}} \{\mathbf{Y}\}_{\text{fluid}}, \quad \{\mathbf{X}\}_{\text{solid}} = [\mathbf{N}]_{\text{solid}} \{\mathbf{Y}\}_{\text{solid}}$$

where

$$\{\mathbf{X}\}_{\text{fluid}} = \{v_r(r)v_\theta(r)v_z(r)T_{rr}(r)T_{r\theta}(r)T_{rz}(r)\}^T, \\ \{\mathbf{Y}\}_{\text{fluid}} = \{ABC\}^T$$

$$[\mathbf{N}]_{\text{fluid}} = \begin{pmatrix} v_1(r) & v_2(r) & v_3(r) \\ v_4(r) & v_5(r) & v_6(r) \\ v_7(r) & 0 & v_8(r) \\ T_1(r) & T_2(r) & T_3(r) \\ T_4(r) & T_5(r) & T_6(r) \\ T_7(r) & T_8(r) & T_9(r) \end{pmatrix}$$

$$\{\mathbf{X}\}_{\text{solid}} = \{u_r(r) u_\theta(r) u_z(r) \sigma_{rr}(r) \sigma_{r\theta}(r) \sigma_{rz}(r)\}^T,$$

$$\{\mathbf{Y}\}_{\text{solid}} = \{A_1 A_2 B_1 B_2 C_1 C_2\}^T$$

$$[\mathbf{N}]_{\text{solid}} = \begin{pmatrix} U_1(r) & U_2(r) & U_3(r) & U_4(r) & U_5(r) & U_6(r) \\ V_1(r) & V_2(r) & V_3(r) & V_4(r) & V_5(r) & V_6(r) \\ W_1(r) & W_2(r) & 0 & 0 & W_3(r) & W_4(r) \\ S_1(r) & S_2(r) & S_3(r) & S_4(r) & S_5(r) & S_6(r) \\ P_1(r) & P_2(r) & P_3(r) & P_4(r) & P_5(r) & P_6(r) \\ X_1(r) & X_2(r) & X_3(r) & X_4(r) & X_5(r) & X_6(r) \end{pmatrix}$$

Coefficients of the corresponding displacement components and the corresponding velocity components in the radial, circumferential and axial directions Eqs. (15) and (19) for fluid domain:

$$\begin{aligned} v_1(r) &= I'_n(k_\phi r) \\ v_2(r) &= -\frac{n}{r} J_n(k_\psi r) \\ v_3(r) &= k_z J'_n(k_\psi r) \\ v_4(r) &= \frac{n}{r} I_n(k_\phi r) \\ v_5(r) &= -J'_n(k_\psi r) \\ v_6(r) &= \frac{nk_z}{r} J_n(k_\psi r) \\ v_7(r) &= -k_z I_n(k_\phi r) \\ v_8(r) &= k_\psi^2 J_n(k_\psi r) \end{aligned}$$

for solid domain:

$$\begin{aligned} (U_1, U_2)(r) &= (I'_n, K'_n)(k_\phi r) \\ (U_3, U_4)(r) &= -\frac{n}{r} (I_n, K_n)(k_\psi r) \\ (U_5, U_6)(r) &= k_z (I'_n, K'_n)(k_\psi r) \\ (V_1, V_2)(r) &= \frac{n}{r} (I_n, K_n)(k_\phi r) \\ (V_3, V_4)(r) &= -(I'_n, K'_n)(k_\psi r) \\ (V_5, V_6)(r) &= \frac{nk_z}{r} (I_n, K_n)(k_\psi r) \\ (W_1, W_2)(r) &= -k_z (I_n, K_n)(k_\phi r) \\ (W_3, W_4)(r) &= -k_\psi^2 (I_n, K_n)(k_\psi r) \end{aligned}$$

Coefficients of the pertinent stress components Eqs. (16) and (20): for fluid domain:

$$T_1(r) = 2\eta \left[I''_n(k_\phi r) - \left(k_\phi^2 - k_z^2 + \frac{\alpha^2}{2} \right) I_n(k_\phi r) \right]$$

$$T_2(r) = -\frac{2\eta n}{r^2} [r J'_n(k_\psi r) - J_n(k_\psi r)]$$

$$T_3(r) = 2\eta k_z J''_n(k_\psi r)$$

$$T_4(r) = \frac{2\eta n}{r^2} [r I'_n(k_\phi r) - I_n(k_\phi r)]$$

$$T_5(r) = -2\eta \left[J''_n(k_\psi r) + \frac{k_\psi^2}{2} J_n(k_\psi r) \right]$$

$$T_6(r) = \frac{2\eta nk_z}{r^2} [r J'_n(k_\psi r) - J_n(k_\psi r)]$$

$$T_7(r) = -2\eta k_z I'_n(k_\phi r)$$

$$T_8(r) = \frac{\eta nk_z}{r} J_n(k_\psi r)$$

$$T_9(r) = \eta (k_\psi^2 - k_z^2) J'_n(k_\psi r)$$

for solid domain:

$$(S_1, S_2)(r) = \left[2\mu \left(I''_n, K''_n \right) + \frac{\lambda v^2 \alpha^4}{2\mu c_1^2} (I_n, K_n) \right] (k_\phi r)$$

$$(S_3, S_4)(r) = \frac{2\mu n}{r^2} [(I_n, K_n) - r(I'_n, K'_n)](k_\psi r)$$

$$(S_5, S_6)(r) = 2\mu k_z (I''_n, K''_n)(k_\psi r)$$

$$(P_1, P_2)(r) = \frac{2\mu n}{r^2} [r(I'_n, K'_n) - (I_n, K_n)](k_\phi r)$$

$$(P_3, P_4)(r) = \mu [k_\psi^2 (I_n, K_n) - 2(I''_n, K''_n)](k_\psi r)$$

$$(P_5, P_6)(r) = \frac{2\mu nk_z}{r^2} [r(I'_n, K'_n) - (I_n, K_n)](k_\psi r)$$

$$(X_1, X_2)(r) = -2\mu k_z (I'_n, K'_n)(k_\phi r)$$

$$(X_3, X_4)(r) = \frac{\mu nk_z}{r} (I_n, K_n)(k_\psi r)$$

$$(X_5, X_6)(r) = -\mu (k_\psi^2 + k_z^2) (I'_n, K'_n)(k_\psi r)$$

The matrix $[\mathbf{M}]$ in Eq. (24) is defined as follows:

$$[\mathbf{M}] = [\mathbf{M}_{11}, \mathbf{M}_{21}, \mathbf{M}_{31}, \mathbf{M}_{41}, \mathbf{M}_{51}, \mathbf{M}_{61}, \mathbf{M}_{71}, \mathbf{M}_{81}, \mathbf{M}_{91}]^T$$

where

$$\begin{aligned} \mathbf{M}_{11} &= \{M_{11}, M_{12}, M_{13}, M_{14}, M_{15}, M_{16}, M_{17}, M_{18}, M_{19}\} \\ \mathbf{M}_{21} &= \{M_{21}, M_{22}, M_{23}, M_{24}, M_{25}, M_{26}, M_{27}, M_{28}, M_{29}\} \\ \mathbf{M}_{31} &= \{M_{31}, 0, M_{33}, M_{34}, M_{35}, 0, 0, M_{38}, M_{39}\} \\ \mathbf{M}_{41} &= \{M_{41}, M_{42}, M_{43}, M_{44}, M_{45}, M_{46}, M_{47}, M_{48}, M_{49}\} \\ \mathbf{M}_{51} &= \{M_{51}, M_{52}, M_{53}, M_{54}, M_{55}, M_{56}, M_{57}, M_{58}, M_{59}\} \\ \mathbf{M}_{61} &= \{M_{61}, M_{62}, M_{63}, M_{64}, M_{65}, M_{66}, M_{67}, M_{68}, M_{69}\} \\ \mathbf{M}_{71} &= \{0, 0, 0, M_{74}, M_{75}, M_{76}, M_{77}, M_{78}, M_{79}\} \\ \mathbf{M}_{81} &= \{0, 0, 0, M_{84}, M_{85}, M_{86}, M_{87}, M_{88}, M_{89}\} \\ \mathbf{M}_{91} &= \{0, 0, 0, M_{94}, M_{95}, M_{96}, M_{97}, M_{98}, M_{99}\} \end{aligned}$$

and whose elements are given by

$$\begin{aligned} (M_{11}, M_{12}, M_{13}) &= (v_1, v_2, v_3)(R_1) \\ (M_{14}, M_{15}, M_{16}, M_{17}, M_{18}, M_{19}) &= -v\alpha^2 (U_1, U_2, U_3, U_4, U_5, U_6)(R_1) \\ (M_{21}, M_{22}, M_{23}) &= (v_4, v_5, v_6)(R_1) \\ (M_{24}, M_{25}, M_{26}, M_{27}, M_{28}, M_{29}) &= -v\alpha^2 (V_1, V_2, V_3, V_4, V_5, V_6)(R_1) \end{aligned}$$

$$\begin{aligned}
(M_{31}, M_{33}) &= (v_7, v_8)(R_1) \\
(M_{34}, M_{35}, M_{38}, M_{39}) &= -v\alpha^2(W_1, W_2, W_3, W_4)(R_1) \\
(M_{41}, M_{42}, M_{43}) &= (T_1, T_2, T_3)(R_1) \\
(M_{44}, M_{45}, M_{46}, M_{47}, M_{48}, M_{49}) &= -(S_1, S_2, S_3, S_4, S_5, S_6)(R_1) \\
(M_{51}, M_{52}, M_{53}) &= (T_4, T_5, T_6)(R_1) \\
(M_{54}, M_{55}, M_{56}, M_{57}, M_{58}, M_{59}) &= -(P_1, P_2, P_3, P_4, P_5, P_6)(R_1) \\
(M_{61}, M_{62}, M_{63}) &= (T_7, T_8, T_9)(R_1) \\
(M_{64}, M_{65}, M_{66}, M_{67}, M_{68}, M_{69}) &= -(X_1, X_2, X_3, X_4, X_5, X_6)(R_1) \\
(M_{74}, M_{75}, M_{76}, M_{77}, M_{78}, M_{79}) &= (S_1, S_2, S_3, S_4, S_5, S_6)(R_2) \\
(M_{84}, M_{85}, M_{86}, M_{87}, M_{88}, M_{89}) &= (P_1, P_2, P_3, P_4, P_5, P_6)(R_2) \\
(M_{94}, M_{95}, M_{96}, M_{97}, M_{98}, M_{99}) &= (X_1, X_2, X_3, X_4, X_5, X_6)(R_2)
\end{aligned}$$

REFERENCES

- [1] H. Lamb, On the velocity of sound in a tube, as affected by the elasticity of the walls, Manchester Literary Philos. Soc. Mem. Proc. 42 (1898) 1–16.
- [2] J.R. Womersley, Oscillatory motion of a viscous liquid in a thin-walled elastic tube: the linear approximation for long waves, Philos. Mag. 46 (1955) 199–219.
- [3] R.H. Cox, Wave propagation through a Newtonian fluid contained within a thick-walled viscoelastic tube, Biophys. J. 8 (1968) 691–709.
- [4] K.D. Mahrer, F.J. Mauk, Seismic wave motion for a new model of hydraulic fracture with an induced low-velocity zone, J. Geophys. Res 92 (B9) (1987) 9293–9309.
- [5] J. Dvorkin, G. Mavko, A. Nur, The dynamics of viscous compressible fluid in a fracture, Geophysics 57 (5) (1992) 720–726.
- [6] A.S. Ashour, Wave motion in a viscous fluid-filled fracture, Int. J. Eng. Sci. 38 (2000) 505–515.
- [7] F. Behroozi, Fluid viscosity and the attenuation of surface waves: a derivation based on conservation of energy, Eur. J. Phys. 25 (2004) 115–122.
- [8] C.Y. Wang, L.C. Zhang, Circumferential vibration of microtubules with long axial wavelength, J. Biomech. 41 (2008) 1892–1896.
- [9] O. San, A.E. Staples, Dynamics of pulsatile flows through elastic microtubes, Int. J. Appl. Mech. 4 (1) (2012) 1250006 (23 pages).
- [10] Y.Z. Wang, H.T. Cui, F.M. Li, K. Kishimoto, Effects of viscous fluid on wave propagation in carbon nanotubes, Phys. Lett. A 375 (2011) 2448–2451.
- [11] E.M. Abulwafa, E.K. El-Shewy, A.A. Mahmoud, Time fractional effect on pressure waves propagating through a fluid filled circular long elastic tube, Egypt. J. Basic Appl. Sci. 3 (2016) 35–43.
- [12] X. Zhou, Vibration and stability of ring-stiffened thin-walled cylindrical shells conveying fluid, Acta Mech. Solida Sin. 25 (2) (2012) 168–176.
- [13] Z. Zhang, Y. Liu, B. Li, Free vibration analysis of fluid-conveying carbon nanotube via wave method, Acta Mech. Solida Sin. 27 (6) (2014) 626–634.
- [14] Z. Zhang, Y. Liu, H. Zhao, W. Liu, Acoustic nanowave absorption through clustered carbon nanotubes conveying fluid, Acta Mech. Solida Sin. 29 (3) (2016) 257–270.
- [15] M. Hosseini, R. Bahaadini, Size dependent stability analysis of cantilever micro-pipes conveying fluid based on modified strain gradient theory, Int. J. Eng. Sci. 101 (2016) 1–13.
- [16] V. Korneev, Slow waves in fractures filled with viscous fluid, Geophysics 73 (1) (2008), doi:10.1190/1.2802174.
- [17] L.D. Landau, E.M. Lifshitz, Fluid Mechanics, Pergamon Press, 1959.
- [18] M. Morse, H. Feshbach, Methods of Theoretical Physics, McGraw-Hill, New York, 1946.
- [19] J.D. Achenbach, Wave Propagation in Elastic Solids, North-Holland, The Netherlands, 1975.
- [20] K.F. Graff, Wave Motion in Elastic Solids, Dover Publications, New York, 1975.
- [21] Comsol Multiphysics, Analysis User's Manual Version 5.2, 2016.